

Large-Scale Poloidal Magnetic Field Dynamo Leads to Powerful Jets in GRMHD Simulations of Black Hole Accretion with Toroidal Field

M.T.P. Liska¹, A. Tchekhovskoy^{2,3}, E. Quataert³

¹*Anton Pannekoek Institute for Astronomy, University of Amsterdam, Science Park 904, 1098 XH Amsterdam, The Netherlands*

²*Center for Interdisciplinary Exploration & Research in Astrophysics (CIERA), Physics & Astronomy, Northwestern University, Evanston, IL 60208, USA*

³*Departments of Astronomy and Physics, Theoretical Astrophysics Center, University of California Berkeley, Berkeley, CA 94720-3411, USA*

Accepted. Received; in original form

ABSTRACT

Accreting black holes launch relativistic collimated jets, across many decades in luminosity and mass, suggesting the jet launching mechanism is universal, robust and scale-free. Theoretical models and general relativistic magnetohydrodynamic (GRMHD) simulations indicate that the key jet-making ingredient is large-scale poloidal magnetic flux. However, its origin is uncertain, and it is unknown if it can be generated in situ or dragged inward from the ambient medium. Here, we use the GPU-accelerated GRMHD code *H-AMR* to study global 3D black hole accretion at unusually high resolutions more typical of local shearing box simulations. We demonstrate that accretion disc turbulence in a radially-extended accretion disc can generate large-scale poloidal magnetic flux in situ, even when starting from a purely toroidal magnetic field. The flux accumulates around the black hole till it becomes dynamically-important, leads to a magnetically arrested disc (MAD), and launches relativistic jets that are more powerful than the accretion flow. The jet power exceeds that of previous GRMHD toroidal field simulations by a factor of 10,000. The jets do not show significant kink or pinch instabilities, accelerate to $\gamma \sim 10$ over 3 decades in distance, and follow a collimation profile similar to the observed M87 jet.

Key words: accretion, accretion discs – black hole physics – MHD – galaxies: jets – methods: numerical

1 INTRODUCTION

Black holes (BHs) can launch relativistic jets through the conversion of BH spin energy into Poynting flux (Blandford & Znajek 1977). The ratio of jet power to accretion power, or jet efficiency, is maximum when the BH is both rapidly spinning and has accumulated a substantial amount of large-scale poloidal (i.e., confined to a meridional, R – z plane) magnetic flux on the event horizon (see e.g. Blandford & Znajek 1977; Komissarov 2001; Tchekhovskoy et al. 2010, 2011). In the presence of a large poloidal magnetic flux, a magnetically arrested disc (MAD) can form (e.g. Narayan et al. 2003; Igumenshchev et al. 2003). The resulting jet efficiency can exceed 100% for geometrically-thick accretion discs (Tchekhovskoy et al. 2011; Tchekhovskoy & McKinney 2012; McKinney et al. 2012) and reach 20% for geometrically-thin discs with an aspect ratio $h/r = 0.03$ (Liska et al. 2018b, in preparation).

One way of obtaining the large-scale poloidal magnetic flux near the BH is advecting it from large radii. While for geometrically thick discs this is expected to readily happen over short distances (as confirmed by 3D GRMHD simulations, e.g., Hawley & Krolik 2006; Tchekhovskoy et al. 2011), it is unclear whether an accretion disc is capable of dragging in the poloidal flux from the ambient medium over 5–6 orders of magnitude in distance all the way down to the BH. This is particularly uncertain given that in many systems

the accretion discs at large radii are expected to cool radiatively and become geometrically-thin. In such discs the poloidal magnetic flux may diffuse out faster than it can be advected inwards (Lubow et al. 1994; however, inward transport of the magnetic flux by disc surface layers might help in alleviating this problem, Rothstein & Lovelace 2008; Guilet & Ogilvie 2012, 2013).

Another way of getting large-scale poloidal magnetic flux on the BH is generating it in situ through a turbulent dynamo (Brandenburg et al. 1995) powered by the magnetorotational instability (MRI, see Balbus & Hawley 1991; Balbus & Hawley 1998). Local shearing box studies found that the dynamo can produce radial and toroidal magnetic fluxes on the scale of the box (e.g., Brandenburg et al. 1995; Stone et al. 1996; Lesur & Ogilvie 2008; Davis et al. 2010; Simon et al. 2012; Salvesen et al. 2016b; Shi et al. 2016; Ryan et al. 2017). However, persistent jets lasting an accretion time require poloidal magnetic flux on a much larger scale. Additionally, the often used quasi-periodic boundary conditions in the horizontal direction imply that the net vertical magnetic flux through the box cannot change in time: in fact, it is a crucial externally-imposed parameter. Shearing box simulations without net flux do not appear to be able to generate poloidal magnetic flux that would affect the turbulence in the same way as the net flux does (Pessah et al. 2007; Bai & Stone 2013; Salvesen et al. 2016a,b; Bhat et al. 2016).

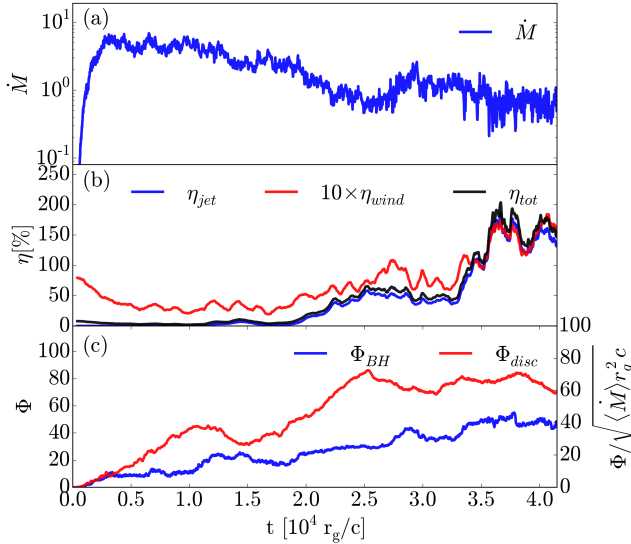


Figure 1. Time evolution of various quantities. (a) The mass accretion rate \dot{M} peaks at early times and gradually decreases; (b) The jets start out much weaker than the disc wind, $\eta_{jet} \ll \eta_{wind}$. However, the two become comparable at $t = (1.2\text{--}1.8) \times 10^4 r_g$, and at later times the situation reverses. Eventually, η_{jet} exceeds 100%, i.e., jet power exceeds the accretion power. (c) This increase in jet power comes from the increase in the strength of BH poloidal magnetic flux, Φ_{BH} , due to the BH accreting dynamo-generated poloidal magnetic flux. Eventually, Φ_{BH} approaches a critical dimensionless value, $\Phi / (\langle \dot{M} \rangle r_g^2 c)^{1/2} \sim 50$, as seen from the right axis that shows the BH flux normalized by the late-time value of $\langle \dot{M} \rangle \approx 0.7$ (Tchekhovskoy et al. 2011). Beyond this point, Φ_{BH} becomes dynamically important and leads to a MAD. A reservoir of positive poloidal magnetic flux Φ_{disc} remains in the disc and may reach the BH at later times.

Free from these limitations, global GRMHD simulations are particularly attractive for studying the formation of large-scale poloidal magnetic flux and the associated jets and outflows. Most global simulations have focused on the initial seed poloidal magnetic flux, in the form of one or several poloidal magnetic field loops; and those show no signs of a large-scale poloidal magnetic flux dynamo (e.g., McKinney 2006; Hawley & Krolik 2006; Shafee et al. 2008; Noble et al. 2009; Penna et al. 2010; Narayan et al. 2012). Beckwith et al. (2008) found that jets formed only for initial conditions with net poloidal magnetic flux, and no jets formed for a purely toroidal initial magnetic flux. For a similar toroidal magnetic field initial condition, but for a larger initial torus, McKinney et al. (2012) found short-lived jets with duration $\lesssim 12 M_{BH} / (10^8 M_\odot)$ days and a low duty cycle, $\sim 2\%$, where M_{BH} is BH mass. Their low time-average efficiency, $\lesssim 0.01\%$, implied that such weak jets would disrupt easily through the kink instability (Liska et al 2018c; Tchekhovskoy & Bromberg 2016; Bromberg & Tchekhovskoy 2016). This low efficiency also appears insufficient to account for feedback from AGN jets on kiloparsec scales (e.g. Fabian 2012) and for the substantial jet power inferred in AGN jets (see, e.g., Prieto et al. 2016 for M87, Nemmen & Tchekhovskoy 2015 for low-luminosity AGN, and Ghisellini et al. 2014 for blazars). Thus, there appears to be a serious mismatch between theory and observations due to the inability of GRMHD simulations to generate sufficient large-scale poloidal magnetic flux starting without one initially.

Yet, it is the toroidal magnetic flux – not the poloidal one – that is a natural starting point for accretion discs in various contexts. In compact object mergers, the orbital shear is expected to produce

a toroidally-dominated magnetic field geometry. In X-ray binaries, the stream overflowing the Roche lobe (or wind from the companion star) would stretch out in the toroidal and radial directions as it feeds the outer disc, and the disc shear would then substantially amplify the toroidal component. Similarly, the tidal debris stream feeding the supermassive BH during a tidal disruption event (TDE) is also expected to lead to a toroidally-dominated magnetic field.

This motivates our current study of BH accretion seeded with purely a toroidal magnetic flux. In Sec. 2 we describe the numerical setup, in Sec. 3 we present our results, and in Sec. 4 we conclude.

2 NUMERICAL APPROACH AND PROBLEM SETUP

We use the H-AMR code (Liska et al. 2018) that evolves the GRMHD equations of motion (Gammie et al. 2003) on a spherical polar-like grid in Kerr-Schild coordinates, using PPM spatial reconstruction (Colella & Woodward 1984) and a 2nd order time-stepping. H-AMR includes GPU acceleration and advanced features, such as adaptive mesh refinement (AMR) and local adaptive timestepping.

Our initial conditions include a rapidly spinning BH of dimensionless spin $a = 0.9$ embedded into an equilibrium hydrodynamic torus with a sub-Keplerian angular momentum profile, $\ell \propto r^{1/4}$, inner edge at $r_{in} = 6r_g$, density maximum at $r_{max} = 13.792r_g$, and outer edge at $r_{out} = 4 \times 10^4 r_g$ (Chakrabarti 1985; De Villiers & Hawley 2003), where $r_g = GM_{BH}/c^2$ is the gravitational radius. The torus scale height ranges from $h/r = 0.2$ at r_{max} to 0.5 at r_{out} . We insert into the torus toroidal magnetic field with a uniform plasma $\beta = p_{gas}/p_{mag} = 5$ and randomly perturb the thermal pressure at the level of 5% to seed the non-axisymmetric MRI.

Operating in spherical polar coordinates, with a logarithmically-spaced r -grid and uniform θ - and ϕ -grids, we use transmissive boundary conditions (BCs) at the poles, $\sin \theta = 0$ (see the supplementary information [SI] in Liska et al. 2018), periodic BCs in the ϕ -direction, and absorbing BCs at the inner and outer radial boundaries, located just inside of the event horizon and at $r = 10^5 r_g$, respectively (thus, both radial boundaries are causally disconnected from the accretion flow). We use a resolution of $N_r \times N_\theta \times N_\phi = 1872 \times 624 \times 1024$, resulting in 70–90 cells per disc scale height, $h/r \approx 0.35\text{--}0.45$. Such high resolution is typically reserved for local shearing box simulations. We then reduce the ϕ -resolution near the pole (at $\sin \theta < 0.5$, using 4 AMR levels, from $N_\phi = 1024$ at equator to $N_\phi = 128$ at the poles) to increase the timestep and maintain a near-unity cell aspect ratio everywhere.

3 RESULTS

Our torus starts out with a purely toroidal magnetic field. Shear causes the field to go unstable to the toroidal MRI, which leads to magnetized turbulence and viscous stresses, driving accretion of gas on to the BH. Figure 1(a) shows that the gas reaches the BH at $t \sim 600 r_g/c$, and mass accretion rate saturates at $t \gtrsim 3,000 r_g/c$ and remains approximately constant until $t \sim 10^4 r_g/c$. Figure 1(b) shows that at this time the only outflow present is a sub-relativistic wind with energy efficiency $\eta_{wind} \approx 5\%$. Figure 1(c) shows that the poloidal magnetic flux on the BH, $\Phi_{BH} = 0.5 \int_{r=r_H} |B^r| dA_{\theta\phi}$, grows from 0 to 20, as shown by the blue line. Here, the integral is over both hemispheres of the event horizon, $r_H = r_g [1 + (1 - a^2)^{1/2}]$, and the factor of 0.5 converts it to one hemisphere (Tchekhovskoy et al. 2011). The reservoir of positive poloidal magnetic flux in the disc, $\Phi_{disc} = \max_r \Phi_p(r)$ with $\Phi_p(r) = \max_\theta \int_0^\theta B^r dA_{\theta\phi}$, shown with

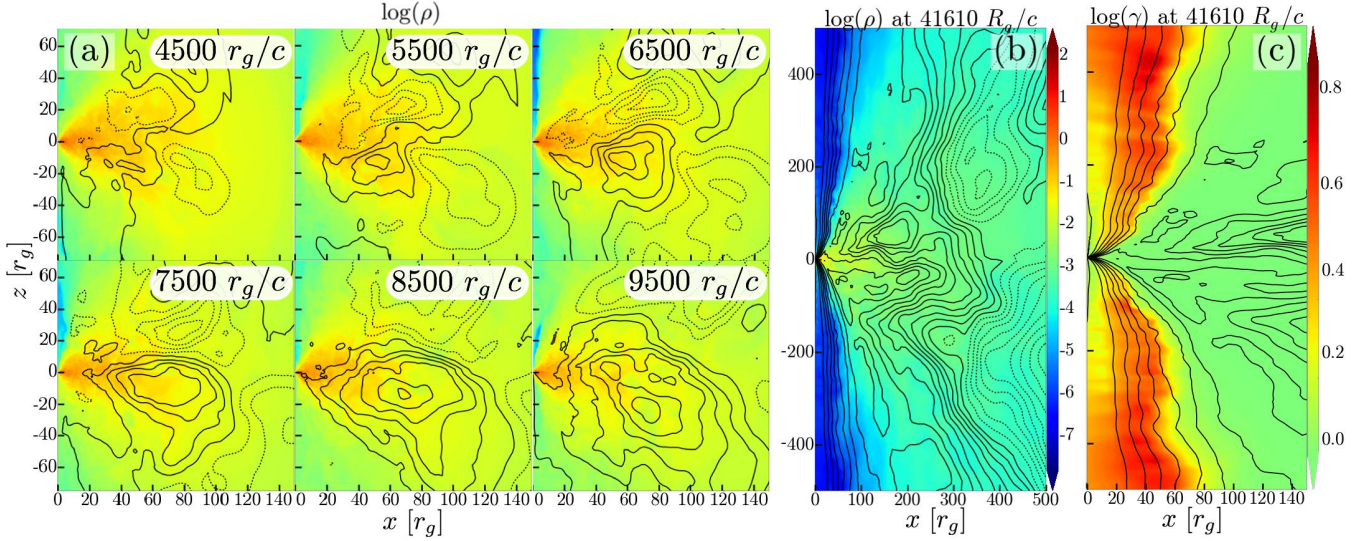


Figure 2. (a) A sequence of meridional slices through the simulation at the approximate times shown, illustrating the development of large scale poloidal flux loops, shown with black lines, of size comparable to the disc thickness, plotted over the density distribution, shown in colour (see the colour bar in panel a). The loops form slightly offset from the equator and buoyantly rise away from it, as expected in an α - Ω dynamo. Initially, several poloidal field loops of positive (solid lines) and negative (dotted lines) polarity stochastically form. However, most of them get expelled, and one largest, lucky, loop takes over. See SI and [this link](#) for a movie. (b) The final snapshot of the simulation, at $t = 4.2 \times 10^4 r_g/c$, revealing two large-scale dynamo-generated poloidal flux loops: their size, $l \gtrsim 100 r_g$, vastly exceeds that of the event horizon, and the loops present themselves to the BH as large-scale poloidal flux. (c) This large-scale flux leads to the launching of persistent relativistic jets with a typical spine-sheath structure, as seen in a colour map of the Lorentz factor, γ . These jets appear stable against global kink and pinch modes at $z \lesssim 2000 r_g$ and readily accelerate to $\gamma \sim 10$.

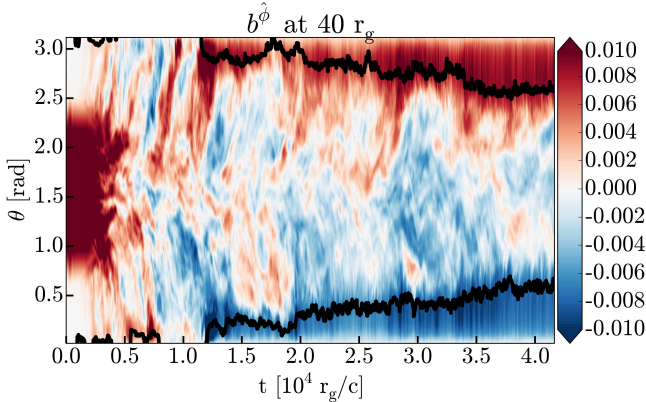


Figure 3. The space-time diagram of toroidally averaged rest-frame magnetic field b^ϕ at $r = 40 r_g$ shows a typical butterfly pattern. Sporadic reversals of disc toroidal magnetic field indicate dynamo activity, albeit an irregular one (see Sec. 3 for detail). Black lines track the disk-jet boundary.

the red line, also keeps growing, pointing to a large-scale dynamo activity in the disc. Figure 2(a) shows a time sequence illustrating the generation of poloidal magnetic flux loops by the MHD turbulence (see the movie in the SI): several loops form just outside the equatorial plane, grow in strength, and buoyantly rise away from the equator. This process is stochastic: one of the loops ends up taking over the inner $100 r_g$ of the disc with the others getting expelled. This is consistent with the α - Ω large-scale poloidal magnetic flux dynamo (Parker 1955; Moffatt 1978), in which a toroidal magnetic field loop undergoes Parker instability, buoyantly rises, and the Coriolis force twists it into a poloidal magnetic field loop. This way, the α -effect can convert toroidal into poloidal flux. The Ω -effect then does the opposite, shearing out this freshly-generated

poloidal magnetic flux loop into toroidal magnetic flux, and thereby completing the positive feedback cycle. This is a possible mechanism for both the initial formation of the poloidal magnetic flux loops and their subsequent runaway growth in strength and size, as seen in our simulations.

This picture is consistent with the butterfly diagram shown in Fig. 3: patches of toroidal magnetic field, b^ϕ , rise with alternating signs away from the equator. However, our dynamo is rather sporadic and irregular, reminiscent of lower plasma β shearing box simulations (e.g. Bai & Stone 2013; Salvesen et al. 2016b) and global simulations of very thick discs (with $h/r = 0.4$, Hogg & Reynolds 2018) that show similar irregularity and even complete absence of sign flips. Most global simulations at high β values tend to show a more regular behavior of the butterfly diagram (Shi et al. 2010; O’Neill et al. 2011; Flock et al. 2012; Beckwith et al. 2011; Simon et al. 2011, 2012; Jiang et al. 2017; Siegel & Metzger 2018). Note the clear asymmetry in our diagram: the upper half is dominated by the positive and the lower half by the negative b^ϕ . This tends to match the polarity of the two jets, demarcated by the black lines, potentially reflecting the fact that the disc and jets are permeated by the same dynamo-generated poloidal magnetic flux loop.

Figure 1(c), right axis, shows that the magnetic flux keeps growing until it approaches a dimensionless value $\Phi/(\langle \dot{M} \rangle r_g^2 c)^{1/2} \approx 50$ (Tchekhovskoy et al. 2011), a critical value at which the flux becomes dynamically-important near the BH and violently obstructs accretion to the point that the disc turns MAD (Narayan et al. 2003; Igumenshchev et al. 2003). Figure 1(b) shows that jets reach $\eta_{\text{jet}} \approx 150\%$, comparable to or exceeding 100% : a tell-tale signature of the MAD state. Figure 2(b),(c) shows that the jets collimate against the disc wind, develop a spine-sheath structure, and accelerate to relativistic velocities, reaching Lorentz factors $\gamma \sim 10$ by $r = 2 \times 10^3 r_g$. Jet acceleration and collimation is similar to that in the M87 galaxy (Nakamura & Asada 2013; Mertens et al. 2016).

Figure 4 shows radial profiles of various quantities in the disc. Whereas at early times the magnetic pressure in the disc is mostly subdominant, at later times it comes close to equipartition as characteristic of MADs (McKinney et al. 2012). This leads to relatively high α -viscosity in the disc, with Maxwell and Reynolds stress contributions of $\alpha_M \approx 0.1$ and $\alpha_R \approx 0.01$, respectively. Such high Maxwell stresses are atypical and were only found in the presence of large-scale poloidal magnetic flux threading the disc (McKinney et al. 2012; Bai & Stone 2013; Salvesen et al. 2016b): indeed, while 60% of the poloidal magnetic flux reaches the BH, the disc retains the rest, as seen in Figs. 2(b),(c) and 4(c).

4 DISCUSSION AND CONCLUSIONS

Using global GRMHD simulations, we demonstrate for the first time that a large-scale poloidal magnetic flux dynamo operates in BH accretion discs. Poloidal field loops form in situ, on the length scale $l \lesssim h \sim r$ and slightly offset from the equator, and tend to rise buoyantly. The formation mechanism is consistent with the α - Ω dynamo, which relies on the buoyancy and Coriolis forces to convert toroidal into poloidal magnetic flux (α -effect), and on the disc shear to convert poloidal into toroidal flux (Ω -effect). At the end of the simulation, the largest loops, which supply their flux to the BH, reside at $r \sim 200r_g$ (see Fig. 2b). As accretion drags the flux inward, it presents itself to the BH as a *large-scale poloidal magnetic flux*, whose scale exceeds the local radius by 2 orders of magnitude. The flux accumulates around the BH until it becomes dynamically-important, and leads to a MAD and magnetically-launched jets whose power exceeds the accretion power.

We initialized our simulations with a relatively strong toroidal magnetic field, with plasma $\beta = 5$, to ensure that they resolve the MRI due to both the initial toroidal and dynamo-generated poloidal magnetic fields: we found that the dynamo did not operate in the simulations that formally resolved the former but not the latter. Figure 4(d) shows that the MRI is well-resolved for $r < 1000r_g$, with $Q_{r,\theta} = 10^2$ cells per MRI wavelength in the r -, and θ - and $Q_\phi = 5 \times 10^2$ in the ϕ -direction. Using the same physical setup, same effective θ -resolution near the equator, and 4 times lower ϕ -resolution, resulted in twice as low jet efficiency of 20% at $t = 2.5 \times 10^4 r_g/c$ (obtained with the HARM code at a resolution of $288 \times 128 \times 128$, with the θ -grid focused on the equator and using a toroidal wedge, $\Delta\phi = \pi$). This suggests that for toroidal flux to generate large-scale poloidal flux it is crucial that the MHD turbulence is well-resolved, possibly also with an order unity cell aspect ratio, in all 3 dimensions.

Figure 4(c) shows that the poloidal flux produced in our simulation makes up $\lesssim 15\%$ of the initial toroidal flux, $\Phi_p(r) = \int_0^r B^\theta dA_{r\theta}$, at $r \lesssim 200r_g$; here, the integral is in the r - and θ -directions. This indicates that large-scale toroidal flux might be a prerequisite for the large-scale poloidal flux dynamo to operate. Assuming that the dynamo converts a fixed fraction of toroidal flux into poloidal flux, it will take longer to generate the same poloidal flux for a weaker initial toroidal flux or, equivalently, higher value of plasma β . If the dynamo-generated poloidal magnetic flux is limited by the time available for the dynamo to operate, stagnation points in the disc – where the gas lingers instead of falling in or flying out and where the effective viscosity α_{eff} vanishes – can become centers of poloidal flux generation. Figure 4(b) shows that the radius of the stagnation point changes very slowly: from $65r_g$ at $t = 10^4 r_g/c$ to $100r_g$ at $t = 4 \times 10^4 r_g/c$. The gas flow is directed away from the stagnation point in all directions, and this expanding

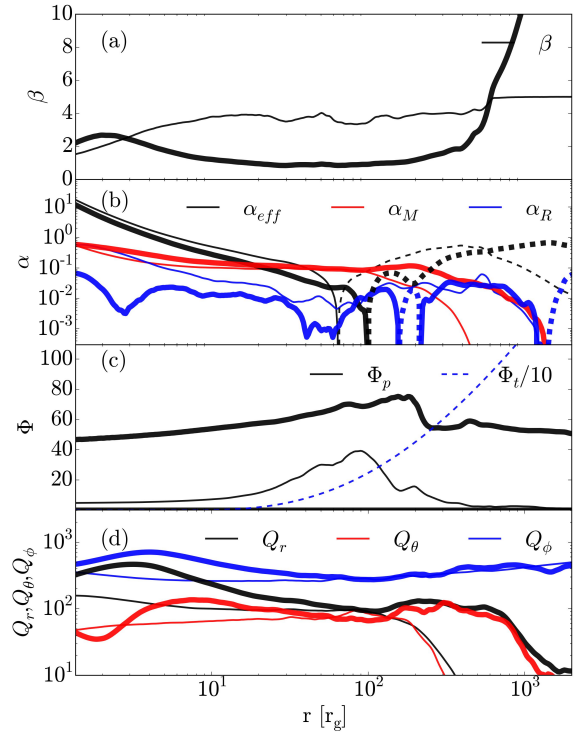


Figure 4. Radial profiles at $t = 10^4 r_g/c$ (thin lines) and $t = 4 \times 10^4 r_g/c$ (thick lines), averaged over $\Delta t = 10^3 r_g/c$. (a) While at early times the magnetic pressure is subdominant, with plasma $\beta \sim 4$, at late times the magnetic pressure reaches equipartition, as the dynamo-generated poloidal magnetic flux increases in strength. (b) The effective viscosity, $\alpha_{\text{eff}} = -v_r v_\phi / c_s^2$, and the contributions to viscosity of Maxwell (α_M) and Reynolds (α_R) stresses. Solid curves show positive and dashed negative values. Maxwell stress dominates over Reynolds stress. Near the BH we have $\alpha_{\text{eff}} > \alpha_M$, likely due to plunging of the gas into the BH. Stagnation points in the flow, where $\alpha_{\text{eff}} = 0$, are favorable locations for dynamo operation (see Sec. 4 for details). (c) The disc has a large reservoir of positive polarity magnetic flux Φ_p , whose peak moves outward with time and which makes up 15% of the initial toroidal magnetic flux Φ_t at $200r_g$, suggesting that even more magnetic flux may be generated at times beyond those simulated. (d) The quality factors, $Q_\#$, the number of cells per MRI wavelength in direction $\#$. Their large values indicate that the turbulence is very well resolved in all three dimensions.

flow pattern assists the dynamo not only in inflating the poloidal flux loop but also in trapping it at the stagnation point. As seen in Figure 2(a), this trapping might be responsible for one lucky loop getting pinned down at the stagnation point, outgrowing the rest of the loops, and dominating the long-term evolution of the system. In a similar way, even for an initial small-scale toroidal magnetic field, a stagnation point may trap a poloidal magnetic flux loop and inflate it to large scales, thereby producing large-scale poloidal magnetic flux. Figure 4(c) shows that in our simulations the peak of the poloidal flux grows in amplitude and moves out to a larger distance, loosely following the movement of the stagnation point. This suggests that the dynamo might indeed benefit from the presence of stagnation points in the flow and that the disc may generate yet more poloidal flux at larger distances from the BH and at later times than simulated in this work. Future simulations will study large-scale poloidal flux dynamo for weaker and smaller-scale initial magnetic flux (toroidal and poloidal) than studied here.

The lack of large-scale poloidal flux generation in global

toroidal field GRMHD simulations till now might stem from a lower field strength considered, lack of stagnation points suitably located in the flow, a limited radial range of the initial toroidal magnetic flux distribution (Beckwith et al. 2008) or a high radial inflow velocity (due to large disc thickness) that may not give the poloidal field loops enough time to grow (McKinney et al. 2012). In the future, it will be important to assess which (if any) of these speculations is correct.

A robust large-scale poloidal flux dynamo can help us understand the prevalence of jets across a wide range of astrophysical systems. Even though typical jet-producing accretion discs are geometrically-thick near the BH, they may be thin at large radii (Esin et al. 1997). Thin discs are thought to be incapable of efficiently transporting large-scale poloidal magnetic flux from the ambient medium to the BH (Lubow et al. 1994; Guilet & Ogilvie 2012, 2013), decreasing the prospects for jet formation. However, if the outer thin disc can transport even just a very weak poloidal magnetic flux, dynamo action in the inner, geometrically-thick disc could amplify the magnetic flux in situ to levels sufficient for forming jets. In some systems the available magnetic flux appears insufficient to account for the observed jet power, such as the jetted TDE Swift J1644+57, for which the stellar magnetic flux falls several orders of magnitude short of that necessary to power the observed jet (Tchekhovskoy et al. 2014; Kelley et al. 2014). The rapid dynamo action we find in this work could help the newly formed TDE accretion disc to amplify the stellar flux to levels sufficient for the production of luminous jets (see also Krolik & Piran 2011).

5 ACKNOWLEDGMENTS

We thank Pallavi Bhat for discussions. This research was made possible by NSF PRAC awards no. 1615281 and OAC-1811605 at the Blue Waters computing project. ML was supported by the NWO Spinoza Prize (PI M.B.M. van der Klis). AT acknowledges support from Northwestern University. This work was supported in part by NSF grants AST 13-33612, AST 1715054, Chandra theory grant TM7-18006X from the Smithsonian Institution, and a Simons Investigator award from the Simons Foundation (EQ).

6 SUPPORTING INFORMATION

Additional Supporting Information may be found in the online version of this article: movie file (link).

REFERENCES

- Bai X.-N., Stone J. M., 2013, *ApJ*, 767, 30
 Balbus S. A., Hawley J. F., 1991, *ApJ*, 376, 214
 Balbus S. A., Hawley J. F., 1998, *Rev. Mod. Phys.*, 70, 1
 Beckwith K., Armitage P. J., Simon J. B., 2011, *MNRAS*, 416, 361
 Beckwith K., Hawley J. F., Krolik J. H., 2008, *ApJ*, 678, 1180
 Bhat P., Ebrahimi F., Blackman E. G., 2016, *MNRAS*, 462, 818
 Blandford R. D., Znajek R. L., 1977, *MNRAS*, 179, 433
 Brandenburg A., Nordlund A., Stein R. F., Torkelsson U., 1995, *ApJ*, 446, 741
 Bromberg O., Tchekhovskoy A., 2016, *MNRAS*, 456, 1739
 Chakrabarti S. K., 1985, *ApJ*, 288, 1
 Colella P., Woodward P. R., 1984, *JCP*, 54, 174
 Davis S. W., Stone J. M., Pessah M. E., 2010, *ApJ*, 713, 52
 De Villiers J.-P., Hawley J. F., 2003, *ApJ*, 589, 458
 Esin A. A., McClintock J. E., Narayan R., 1997, *ApJ*, 489, 865
 Fabian A. C., 2012, *ARA&A*, 50, 455
 Flock M., Dzyurkevich N., Klahr H., Turner N., Henning T., 2012, *ApJ*, 744, 144
 Gammie C. F., McKinney J. C., Tóth G., 2003, *ApJ*, 589, 444
 Ghisellini G., Tavecchio F., Maraschi L., Celotti A., Sbarbato T., 2014, *Nature*, 515, 376
 Guilet J., Ogilvie G. I., 2012, *MNRAS*, 424, 2097
 Guilet J., Ogilvie G. I., 2013, *MNRAS*, 430, 822
 Hawley J. F., Krolik J. H., 2006, *ApJ*, 641, 103
 Hogg J. D., Reynolds C. S., 2018, *ApJ*, 861, 24
 Igumenshchev I. V., Narayan R., Abramowicz M. A., 2003, *ApJ*, 592, 1042
 Jiang Y.-F., Stone J., Davis S. W., 2017, *ArXiv:1709.02845*
 Kelley L. Z., Tchekhovskoy A., Narayan R., 2014, *MNRAS*, 445, 3919
 Komissarov S. S., 2001, *MNRAS*, 326, L41
 Krolik J. H., Piran T., 2011, *ApJ*, 743, 134
 Lesur G., Ogilvie G. I., 2008, *A&A*, 488, 451
 Liska M., Hesp C., Tchekhovskoy A., Ingram A., van der Klis M., Markoff S., 2018, *MNRAS*, 474, L81
 Lubow S. H., Papaloizou J. C. B., Pringle J. E., 1994, *MNRAS*, 267, 235
 McKinney J. C., 2006, *MNRAS*, 368, 1561
 McKinney J. C., Tchekhovskoy A., Blandford R. D., 2012, *MNRAS*, 423, 3083
 Mertens F., Lobanov A. P., Walker R. C., Hardee P. E., 2016, *A&A*, 595, A54
 Moffatt H. K., 1978, *Magnetic field generation in electrically conducting fluids*. Cambridge, England, Cambridge University Press. 353 p.
 Narayan R., Igumenshchev I. V., Abramowicz M. A., 2003, *PASJ*, 55, L69
 Nakamura M., Asada K., 2013, *ApJ*, 775, 118
 Narayan R., Sądowski A., Penna R. F., Kulkarni A. K., 2012, *MNRAS*, 426, 3241
 Nemmen R. S., Tchekhovskoy A., 2015, *MNRAS*, 449, 316
 Noble S. C., Krolik J. H., Hawley J. F., 2009, *ApJ*, 692, 411
 O’Neill S. M., Reynolds C. S., Miller M. C., Sorathia K. A., 2011, *ApJ*, 736, 107
 Parker E. N., 1955, *ApJ*, 122, 293
 Penna R. F., McKinney J. C., Narayan R., Tchekhovskoy A., Shafee R., McClintock J. E., 2010, *MNRAS*, 408, 752
 Pessah M. E., Chan C.-k., Psaltis D., 2007, *ApJ*, 668, L51
 Prieto M. A., Fernández-Ontiveros J. A., Markoff S., Espada D., González-Martín O., 2016, *MNRAS*, 457, 3801
 Rothstein D. M., Lovelace R. V. E., 2008, *ApJ*, 677, 1221
 Ryan B. R., Gammie C. F., Fromang S., Kestener P., 2017, *ApJ*, 840, 6
 Salvesen G., Armitage P. J., Simon J. B., Begelman M. C., 2016, *MNRAS*, 460, 3488
 Salvesen G., Simon J. B., Armitage P. J., Begelman M. C., 2016, *MNRAS*, 457, 857
 Shafee R., McKinney J. C., Narayan R., Tchekhovskoy A., Gammie C. F., McClintock J. E., 2008, *ApJ*, 687, L25
 Shi J., Krolik J. H., Hirose S., 2010, *ApJ*, 708, 1716
 Shi J.-M., Stone J. M., Huang C. X., 2016, *MNRAS*, 456, 2273
 Siegel D. M., Metzger B. D., 2018, *ApJ*, 858, 52
 Simon J. B., Beckwith K., Armitage P. J., 2012, *MNRAS*, 422, 2685
 Simon J. B., Hawley J. F., Beckwith K., 2011, *ApJ*, 730, 94
 Stone J. M., Hawley J. F., Gammie C. F., Balbus S. A., 1996, *ApJ*, 463, 656
 Tchekhovskoy A., Bromberg O., 2016, *MNRAS*, 461, L46
 Tchekhovskoy A., McKinney J. C., 2012, *MNRAS*, 423, L55
 Tchekhovskoy A., Metzger B. D., Giannios D., Kelley L. Z., 2014, *MNRAS*, 437, 2744
 Tchekhovskoy A., Narayan R., McKinney J. C., 2010, *ApJ*, 711, 50
 Tchekhovskoy A., Narayan R., McKinney J. C., 2011, *MNRAS*, 418, L79